BEC-BCS crossover in ultracold Fermionic gas

Wenchao Xu

December 12, 2011

Department of Physics, University of Illinois at Urbana-Champaign, Urbana, IL, 61801

Abstract

By using Feshbach resonance, the atom-atom interaction can be tuned from attractive effect to repulsive, which allows us to study the crossover from Bardeen-Cooper-Schrieffer (BCS) type superfluid with paring in momentum space, to Bose-Einstein condensation (BEC) of bound pairs in real space. In this paper, I will present the mean field approach for both sides at T=0, and then discuss some experimental results in degenerate Fermi gas. Such results demonstrated the existence of these two emergent states and revealed the energy dispersion relationship and momentum distribution for both sides.

1 Introduction

Ultracold atomic or molecular gas provides us a platform to simulate quantum many-body system. The achievement of Bose-Einstein condensation [1, 2], and the realization of Fermi degeneracy [3] in ultracold atoms have opened up a new world where the fundamental behavior of quantum matter can be investigated. Compared with traditional condensed matter physics, the study on ultracold gases has the advantage of controlling on various parameters, providing us a new approach to reveal the mysteries of many-body problems.

One of those many-body problems is the study on BEC-BCS crossover. This problem, first proposed by theorists in condensed matter physics[4, 5], have been brought into focus in ultracold system due to its ability to tune the atom-atom interaction among a large range. Fig. 1 displays a vivid picture to describe this phenomenon. In the BEC limit, two Fermionic atoms form a tightly bound pairs in real space, and they, as a molecule, follow the Bose-Einstein statistics. Thus Bose-Einstein condensate emerges under critical temperature. On the other side, in the BCS limit where the attraction is weak, the pairs show up only in momentum space, just like the Cooper pairs in superconductor.

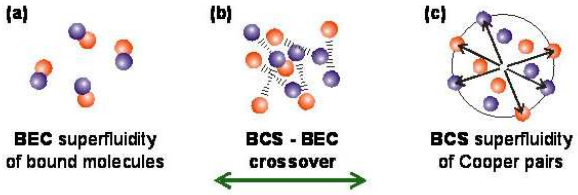

Figure 1: Schematic for BEC-BCS crossover. By tuning the interaction, the Fermionic atoms undergo a crossover from Bose-Einstein condensation (BEC) of bound pairs in real space to Bardeen-Cooper-Schrieffer (BCS) type superfluid with paring in momentum space.

In section 2, I will present the mean-field approach for BEC-BCS crossover at zero temperature. In Section 3, the effect of Feshbach resonance that plays a crucial role in controlling the atom-atom interaction will be discussed. Finally, in Section 4, I will introduce the experiments that demonstrate the existence of these two emergent states, and reveal their energy dispersion relationship.

2 Mean-field approach for BEC-BCS crossover at T=0

Under Bogoliubov transformation,

$$\begin{pmatrix} c^\dagger_{k,\uparrow} \\ c_{-k,\downarrow} \end{pmatrix} = \begin{pmatrix} u_k & -v_k \\ v^*_k & u^*_k \end{pmatrix} \begin{pmatrix} \alpha_{k,\uparrow} \\ \alpha^\dagger_{-k,\downarrow} \end{pmatrix},$$

the so-called BCS Hamiltonian

$$H_{BCS} = \sum_{k\sigma} \xi_k c^\dagger_{k\sigma} c_{k\sigma} + \sum_{kk'} U_{kk'} c^\dagger_{k\uparrow} c^\dagger_{-k\downarrow} c_{k\downarrow} c_{-k\uparrow},$$

becomes

$$H_{BCS} = H_{GS} + \sum_k \varepsilon_k (\alpha^\dagger_{k,\uparrow}\alpha_{k,\uparrow} + \alpha^\dagger_{k,\downarrow}\alpha_{k,\downarrow})$$

where $\xi_k = \frac{\hbar^2 k^2}{2m} - \mu$ and $\varepsilon_k = \sqrt{(\frac{\hbar^2 k^2}{2m} - \mu)^2 + \triangle^2}$. c_k is fermionic annihilation operator. $\triangle_k = -\sum_{k'} U_{kk'} \frac{1}{2\varepsilon_{k'}} \triangle_{k'}$.

The ground state of the system is

$$|\psi_{BCS}\rangle = \prod_k (u_k + v_k c^\dagger_{k\uparrow} c^\dagger_{k\downarrow}) |0\rangle .$$

Notice that

$$\triangle_k = -\sum_{k'} U_{kk'} \frac{1}{2\varepsilon_{k'}} \triangle_{k'} \equiv -UG\triangle,$$

where $U_{kk'}$ on the right side is dependent on k'. Now we want to extract the information about the effective interaction, i.e. to write $\triangle_k$ as $\triangle_k = -U_0 \sum_{k'} G_{k,k'} \triangle_{k'}$, where U_0 is independent of k.

Notice that formally we have $U = U_0 + U_0 \tilde{G} U \approx U_0 + U_0 \tilde{G}_0 U$, where $\tilde{G} = -G_0 = \frac{1}{2\varepsilon^0_k}$, where $\varepsilon^0_k = \frac{\hbar^2 k^2}{2m}$, which is the two-particle propagator in non-interacting Fermion system. Hence we have $U = (1 + U_0 G_0)^{-1} U_0$. As a result

$$\triangle = -UG\triangle = -(1 + U_0 G_0)^{-1} U_0 G \triangle.$$

Multiplying both sides by $(1 + U_0 G_0)$, we find

$$\triangle_k = -U_0 (G + G_0) \triangle_k,$$

or

$$\triangle_k = -U_0 \sum_{k'} (\frac{1}{2\varepsilon_{k'}} - \frac{1}{2\varepsilon^0_k}) \triangle_{k'}. \tag{1}$$

Notice that the expression for $\triangle_k$ is different from the one deduced from phonon interaction in metals. The reason is that Equ. 1 goes beyond the weak-coupling limit, where the contribution from right side only extends over an energy interval near the Fermi surface.

In dilute neutral gas, two-body interaction at long wavelength and low energy dominates. Under Born approximation, $U_0 = \frac{2\pi\hbar^2 a}{m_r}$, where m_r is the reduced mass and equals $\frac{m}{2}$ for indistinguishable Fermionic system. Then we can rewrite Equ. 1 as:

$$\frac{m}{4\pi\hbar^2 a} = \int \frac{d^3 k}{(2\pi)^3} (\frac{1}{2\varepsilon_{k'}} - \frac{1}{2\varepsilon^0_{k'}}), \tag{2}$$

where the summation has been replaced by integral over k.

At the same time, at zero temperature, the total number of particles in this system should satisfy

$$n = \frac{2}{V}\sum_k v_k^2 = \frac{1}{V}\sum_k (1 - \frac{\varepsilon_k^0 - \mu}{\varepsilon_k}) \tag{3}$$

In order to interpret the physical meaning of Equ. 2 and Equ. 3, we first make them dimensionless by scaling energy as $\tilde{\varepsilon} = \varepsilon/\varepsilon_F$, and then we have

$$\int_0^\infty d\tilde{\varepsilon}\tilde{\varepsilon}^{\frac{1}{2}}(\frac{1}{\tilde{\varepsilon}} - \frac{1}{\sqrt{(\tilde{\varepsilon}-\tilde{\mu})^2 + \tilde{\triangle}^2}}) = \pi(k_F a)^{-1} \tag{4}$$

$$\int_0^\infty d\tilde{\varepsilon}\tilde{\varepsilon}^{\frac{1}{2}}(1 - \frac{\tilde{\varepsilon}-\tilde{\mu}}{\sqrt{(\tilde{\varepsilon}-\tilde{\mu})^2 + \tilde{\triangle}^2}}) = \frac{4}{3} \tag{5}$$

To illustrate BEC-BCS crossover, here we would consider the limit situation:

- $(k_F a)^{-1} \to -\infty$. This limit corresponds to the weakly attractive interacting case. As a trail solution, we suppose $\mu \to \varepsilon_F$. Then it turns out for Equ. 5, only the integral around Fermi surface contributes and we obtain $\triangle = \frac{8}{e^2}\epsilon_F e^{-1/N(\epsilon_F)|U_0|}$, in a similar form as the BCS theory predicted in metal.

- $(k_F a)^{-1} \to +\infty$. At this limit, Equ. 4 hints that the chemical potential μ becomes negative. Assuming that $|\mu| \gg \triangle$, which can be verified self-consistently later, we can expand the above equations to the first order in $\triangle^2$. Then Equ. 4 and Equ. 5 become

  $$\int d\tilde{\varepsilon}\tilde{\varepsilon}^{\frac{1}{2}}(\frac{1}{\tilde{\varepsilon}} - \frac{1}{(\tilde{\varepsilon}-\tilde{\mu})^2} + \frac{\triangle^2}{2(\tilde{\varepsilon}-\tilde{\mu})^3}) = \pi(k_F a)^{-1}$$

  and

  $$\int_0^\infty d\tilde{\varepsilon}\tilde{\varepsilon}^{\frac{1}{2}}\frac{\triangle^2}{2(\tilde{\varepsilon}-\tilde{\mu})^2} = \frac{4}{3}.$$

  The latter integral gives us the expression for $\triangle^2$ by μ, then put it into the first integral, we obtain$\triangle \to \frac{4\varepsilon_F}{\sqrt{3\pi}(k_F a)^{\frac{1}{2}}}$ and $\mu \to -\frac{\hbar^2}{2ma^2}$; $\frac{|\mu|}{\triangle} \propto a^{-3/2} \to \infty$. Notice that in this limit, $\mu$is just the half of the binding energy of two atoms, indicating that with the increasing of $(k_F a)^{-1}$, two Fermionic atoms form a bound state and behave like Bosons.

Fig. 2 displays the curves of $\tilde{\mu}$ and $\tilde{\triangle}$ as functions of $(k_F a)^{-1}$, obtained by solving Equ. 4 and Equ.5 self-consistently[6].

Though approximate, the above approach provides the comprehensive argument for BEC-BCS crossover. To involve more factors into consideration, Monte Carlo method is widely used[7], which I will not discuss in this paper. In next two sections, the experimental technique and results on the study of BEC-BCS crossover will be discussed.

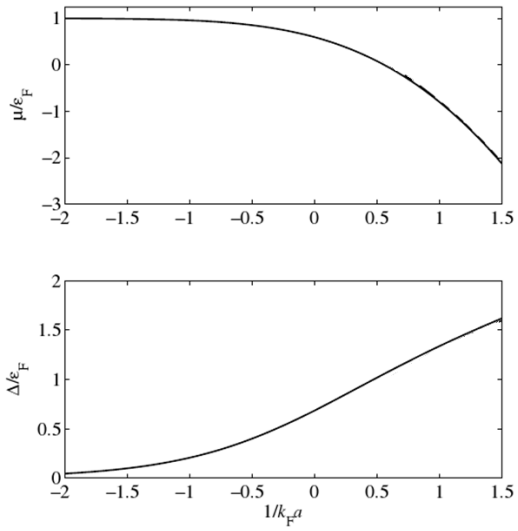

Figure 2: The chemical potential and energy gap at $T = 0$ as functions of $(1/k_F a)^{-1}$. From Ref. [6]

3 Feshbach resonance: tuning the atom-atom interaction

To make the study on BEC-BCS crossover possible, the atom-atom interaction must be tuned within a large range. As a concept coming from nuclear physics, Feshbach resonance now plays a vital role in controlling effective interaction between ultracold atoms, by adjusting an external parameter such as the magnetic field. To illustrate this method in a simple way, we can consider two potential curves as shown in Fig. 3. The open channel cannot support a bound state for particles with energy larger than E_{th}. However, they can form a bound state in the closed channel. If the energy of an open channel matches the energy of bound states in closed channel, there will be a strong mixing between these two channels and the so-called Feshbach resonance will happen. As we will see later, Feshbach resonance is an effect resulted from second-order perturbation.

The origin of these two channels is due to the singlet pairing or triplet pairing of two atoms, analogous to the anti-bonding orbital and bonding orbital in H_2. The inset of Fig. 3 shows the interaction potential vs atomic separation distance for Li_2.

Here we consider a two-body scattering problem, the wavefunction for the relative motion can be written as a sum of incoming plane wave and scattering wave, i.e. $\psi = e^{ikr} + \psi_{sc}$. Under Fourier transformation, the wavefunction can be written as $\psi(k') = (2\pi)^3\delta(k' - k) + \psi_{sc}(k')$. Take this into Schrödinger's equation, we have

$$\psi_{sc}(k') = (\frac{\hbar^2 k^2}{m} - \frac{\hbar^2 k'^2}{m} + i\eta)^{-1}(U_{k',k} + \frac{1}{V}\sum_{k''} U(k', k'')\psi_{sc}(k'')),$$

where $U(k', k'') = \int d^3 r U(r) e^{i(k'-k'')r}$, and η guarantees that the scattering part only includes outgoing waves.

To first order, we have $\psi^1_{sc}(k') = (\frac{\hbar^2 k^2}{m} - \frac{\hbar^2 k'^2}{m} + i\varepsilon)^{-1} U_{k',k}$. In the limit where $k \to 0$ and $r \to \infty$, $\psi_{sc}(k') = -\frac{m}{\hbar^2 k'^2} U_{k'}$

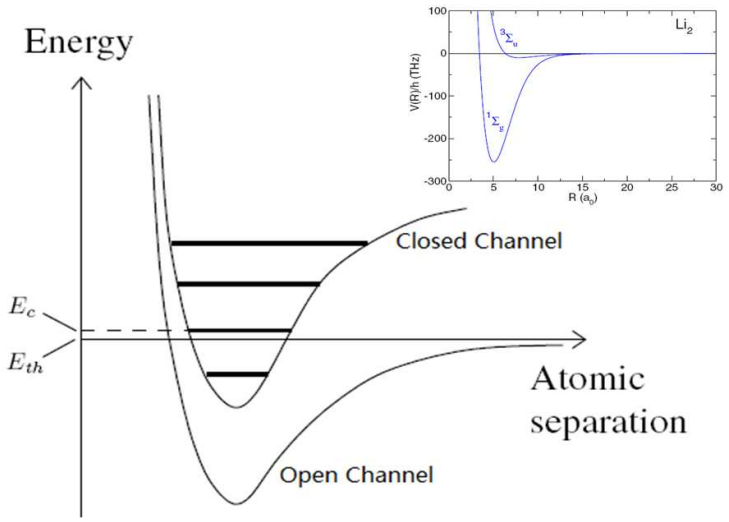

Figure 3: The schematic plot for two-channel model that illustrates the Feshbach resonance. If the energy of bound states E_c in the closed channel (upper) gets close to the threshold energy E_{th} for the open channel (lower), the two channels couple together and introduce strong effective interaction between atoms. The inset is the potential as a function of atomic separation for Li_2(From Ref. [8]).

$$\psi_{sc}(r) = \int \frac{d^3k}{(2\pi)^3}\psi_{sc}(k)e^{ikr} = \int \frac{d^3k}{(2\pi)^3}(-\frac{m}{\hbar^2k^2})\int d^3r'U(r')e^{-ikr'}e^{ikr} = -\frac{m}{4\pi\hbar^2 r}\int drU(r),$$

from which we obtain the scattering length a_0 as

$$a_0 = \frac{m}{4\pi\hbar^2}\int drU(r) \equiv \frac{m}{4\pi\hbar^2}U_0, \tag{6}$$

we could regard U_0 as a renormalized interaction for dilute gas.

Feshbach resonance requires us to consider the second-order perturbation.

$$\psi_{sc}(k') = \psi^1_{sc}(k') + \frac{1}{V}\sum_{k''}U(k^{'},k^{''})\frac{1}{E_k - E_{k''} + i\varepsilon}U(k^{''},k)$$

Then the scattering length becomes

$$\frac{4\pi\hbar^2}{m}a = \frac{4\pi\hbar^2}{m}a_0 + \sum_{k''}\frac{U(k',k'')U(k'',k)}{E_k - E_{k''}},$$

where a_0 is just the scattering length as in Equ. 6.

If E_{th} is close to E_c, the contribution from $\frac{1}{E_{th}-E_c}$ will dominate and the contribution from all other states may be represented by a non-resonant scattering length, denoted as $a_{non-res}$. The expression for scattering length can be rewritten as:

$$\frac{4\pi\hbar^2}{m}a = \frac{4\pi\hbar^2}{m}a_{non-res} + \frac{|\langle\psi_c|U|\psi_{th}\rangle|^2}{E_{th} - E_c}$$

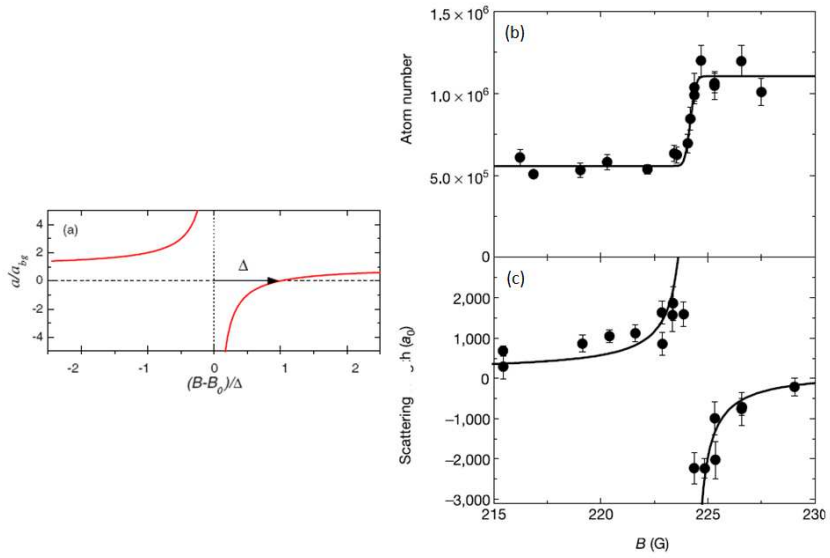

Figure 4: Feshbach resonance. (a): scattering wavelength vs magnetic detuning $B-B_0$ from Feshbach resonance position. From Ref. [8] (b): Experimental measurement of the Feshbach resonance position B_0 for ^{40}K. The curve for atom number vs magnetic field reveals the onset position where the dissociation of molecules happens, from which we obtain $B_0 = 224.18 \pm 0.05G$. (c): Corresponding experimental measurement for scattering wavelength vs magnetic field. From Ref. [9].

With external magnetic field, the value of a can be tuned. Suppose that $E_{th}-E_c$ vanishes for given magnetic field B_0, we can expand it around B_0 to first order, then we have

$$E_{th} - E_c = (\mu_c - \mu_\alpha - \mu_\beta)(B - B_0) + O((B - B_0)^2),$$

where $\mu_\alpha = -\frac{\partial \varepsilon_\alpha}{\partial B}$ and $\mu_\beta = -\frac{\partial \varepsilon_\beta}{\partial B}$ are the magnetic moments for the two atoms in the open channel, and $\mu_c = -\frac{\partial \varepsilon_c}{\partial B}$ is the magnetic moment for the molecular bound state. As a result, the scattering length can be written as

$$a = a_{non-res}(1 - \frac{\triangle}{B - B_0}), \tag{7}$$

where $\triangle = \frac{m}{4\pi\hbar^2 a_{non-res}} \frac{|\langle\psi_c|U|\psi_{th}\rangle|^2}{E_{th}-E_c}$, and corresponding curve for a vs $B - B_0$ is shown in Fig. 4(a).

Hence, by modifying the external magnetic field, we can tune the scattering length from negative to positive. In other word, the effective interaction between atoms varies from attraction to repulsion, provides us the platform to study BEC-BCS crossover. The determination of the position where Feshbach resonance happens plays a vital role in experiments on BEC-BCS crossover. The basic principle is to find out the corresponding magnetic field where the molecules dissociate. For example, Fig. 4(b) is the experimental measurement for Feshbach resonance position in ^{40}K atomic gas.

4 BEC-BCS crossover in experiments

For Fermionic atoms, the total number of the neutrons, protons and electrons should be even, therefore they satisfy the Fermi-Dirac statistics (e.g. ^6Li, ^{40}K). To observe the quantum behavior of atomic gas, it is necessary to cool them down below the degenerate temperature T_F. Though the details of cooling technique may vary for different kinds of atoms, the basic procedure includes laser cooling and subsequent evaporation cooling. After that, the atoms are trapped in an optical dipole trap and further investigation can be conducted.

4.1 Observation of Bose-Einstein condensation of molecules

Usually in the study on BEC-BCS crossover, researchers prepare an mixture of atoms in two different hyperfine states (which can be labeled as $|\uparrow\rangle$ and$|\downarrow\rangle$) at temperature below quantum degeneracy. Then the magnetic field will be applied to modify the effective interaction between atoms. Finally the gas is released from the trap and expands freely; the momentum distribution of atoms can be measured through time-of-flight absorption imaging, as shown in Fig 5. With the reduction of temperature, Fig 5 shows an direct observation of the emergence of molecular Bose-Einstein condensate for ^6Li and ^{40}K, respectively.

Since the original gas cloud in an optical trap is a mixture of unpaired atoms and molecules, one experimental detail we should pay attention to is how to extract the information about molecular condensation. For Fig 5(a), after the optical trap is turned off, a radio frequency pulse is applied to dissociate the molecules into free atoms on other hyperfine states, while the residual unpaired atoms are not affected. Then through spin-selective imaging, the pure information about the molecular condensation can be obtained. Fig 5(b) used another method: they first dissociated the molecules by sweeping the magnetic field up to an intensity far above the Feshbach resonance. Then both the unbound atoms and original molecules are imaged; on the other side, without such magnetic sweep, only the unbound atoms are imaged. The comparison of these two images reveal the information for pure molecular component.

4.2 Observation of condensate on both sides of BEC-BCS crossover

Beyond the extreme BEC region, we could investigate the BEC-BCS crossover. However, measuring the condensate fraction of Fermionic pairs on the BCS side is challenging since it is hard to identify the condensate component. In the work of C. A. Regal et al[12], they pairwise projected the fermionic atoms onto molecules and measured the momentum distribution of the resulting molecular gas. The experimental procedure is illustrated in the inset of Fig. 6. Once the Fermionic gas is released from the trap, the magnetic field is reduced rapidly, to drive the atoms into the BEC side, where the atoms with opposite momentum that form a pair in momentum space combine together to form a bound state with zero momentum. As a result, we can measure the condensate fraction just as in the molecular BEC limit (they excluded the possibility that such condensation was formed during this expansion process rather than at B_{hold}.)

The main result in [12] is shown in Fig. 6 and Fig. 7. Fig. 6 demonstrated the existence of condensate on both sides. Besides, by varying the hold time, we can see that the condensate

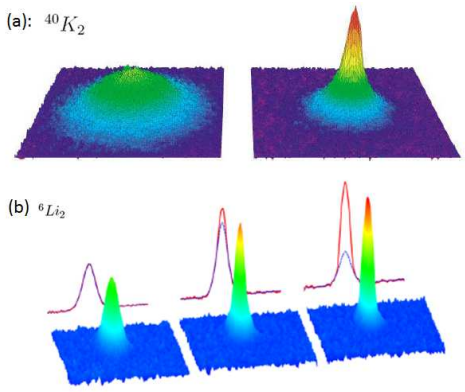

Figure 5: The emergence of molecular BEC in Fermionic ultracold gas. Both are the density distribution observed in time-of-flight absorption images. (a): ^{40}K. From left to right, the temperature is $T/T_F \approx 0.19$ and 0.06. From Ref. [10] (b): $^6Li_2$, together with their axially integrated radial density profiles. From left to right, the initial temperature is $T/T_F \approx 0.2$, 0.1, and 0.05, respectively. From Ref. [11]. They clearly demonstrated the emergence of Bose-Einstein condensation of bound Fermionic pairs.

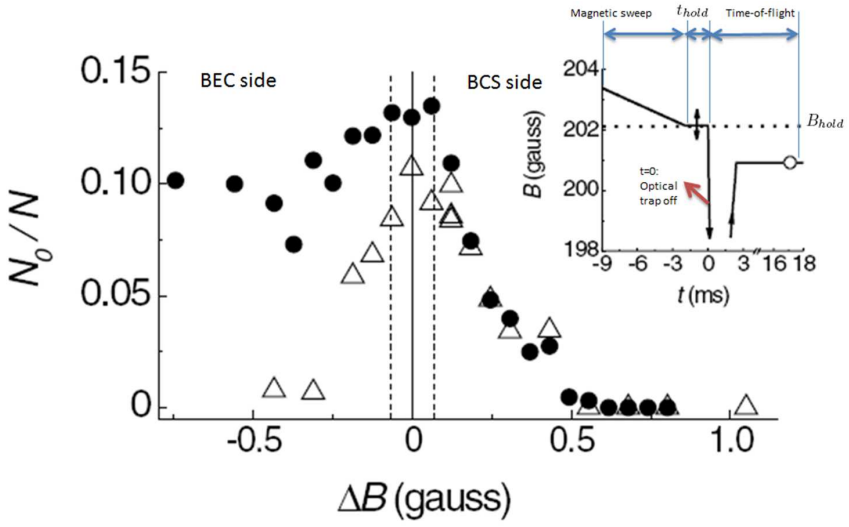

Figure 6: Condensate fraction vs detuning from Feshbach resonance $\triangle B = B_{hold} - B_0$. The hold time is 2ms (for black dots) and 30ms (for white triangles). The inset describes the experimental procedure. The magnetic field sweeps to an intensity around the resonance position, within the region indicated by black two-sided arrow. This process is slow enough to provide sufficient time for atoms and molecules to collide to reach equilibrium. Then they kept this magnetic field for some certain time, called t_{hold}. At the time $t = 0$, the optical trap is turned off and the gas is released. At the same time, the magnetic field is reduced rapidly by 10G, pushing the gas into the BEC side with weak interaction. Reprint from Ref. [12].

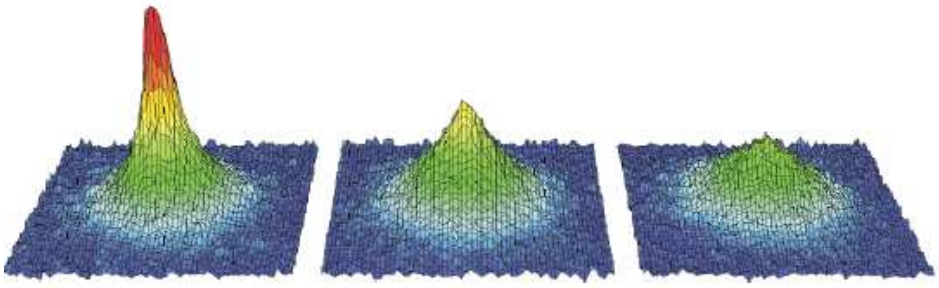

Figure 7: The momentum distribution for fermionic condensate on BCS-side. The images are taken after the pairwise projection of atoms with opposite momentum onto molecules. From left to right, the detuning from Feshbach resonance is $\triangle B = 0.12$, 0.25 and 0.55G. The corresponding condensate fractions are $N_0/N = 0.10$, 0.05 and 0.01, respectively. From Ref. [12].

on the BEC side has relatively long life-time. Fig. 7 displays the momentum distribution for the condensate on the BCS side, after the momentum of atoms are pairwise projected onto a molecular gas. It indicates that the condensate fraction decreases rapidly as the system goes far into the BCS side. It satisfies the conclusion we derived in Section 2. As shown in Fig. 2, the gap energy reduces exponentially as $(k_F a)^{-1} \to -\infty$, and the gas finally behaves like free Fermions.

4.3 Excitation spectroscopy for BEC-BCS crossover

The observation of condensate on the BCS side is not sufficient to reveal their properties. To convince that they have BCS-like behavior, it is necessary to obtain more information, such as their energy dispersion relationship. Momentum-resolved radio-frequency spectroscopy, similar to angle-resolved photoemission spectroscopy (ARPES) widely used in condensed matter physics, allows us to study the single-particle excitation in BEC-BCS crossover. In condensed matter, once the photoelectrons ejected from the sample are collected and counted, their intensity and momentum k can be obtained. Moreover, the original single-particle energy is $E = \frac{\hbar^2 k^2}{2m} + W - hv$, where W is the work function of the surface. Such photoemission spectroscopy provides a lot information about single-particle states. Analogously, for ultracold atomic gas, through a radio-frequency pulse, the atoms are driven into an unoccupied Zeeman spin state, and their momentum can be detected by spin-selective time-of-flight imaging. Since the momentum carried by photon is negligible compared with the momentum of atoms, the momenta of those outcoupled atoms reflect the momentum of original states. Besides, the energy expression is almost the same as the one in condensed matter, except W corresponds to the Zeeman energy splitting.

D. S. Jin's group used this technique to probe the single-particle excitation spectrum in ^{40}K degenerate gas around Feshbach resonance[13]. Fig. 8(a) is the spectroscopy for weakly interacting gas. The intensity, which is proportional to the number of atoms transferred into the untrapped state, is plotted as a function of momentum and energy. The white dots, which mark the centers of the intensity at each momentum k, ,match well with the expected parabolic dispersion as shown in black line. Fig. 8(b) reveals the excitation spectroscopy

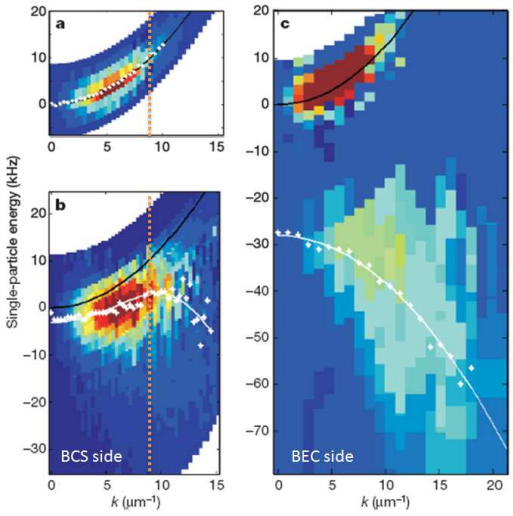

Figure 8: Single-particle excitation spectral for ^{40}K ultracold atomic gas. Black lines are the dispersion curve for an ideal Fermi gas, and the white symbols mark the center of energy distribution for given momentum. (a): very weakly interaction Fermi gas. The Fermi momentum $k_F = 8.6 \pm 0.3 \mu m^{-1}$, as plotted by orange dots. (b): strongly interacting Fermi gas on the BCS side. The white line is a fit to BCS-like dispersion. (c): Fermi gas on the BEC side. The upper feature results from unpaired atoms and the lower feature comes from molecules. The white line is a fit by quadratic dispersion with an energy shift. Reprint from Ref. [13].

where $(k_F a)^{-1} \approx 0$. It clearly reveals a pairing energy gap; the experimental data are fit to a BCS-like dispersion curve, i.e. $E = \mu - \sqrt{(\varepsilon_k - \mu)^2 - \triangle^2}$. Fig. 8(c) is far on the BEC-side ($(k_F a)^{-1} \gg 1$), where the pairing in momentum space becomes a two-body binding in real space. There are two branches in Fig. 8(c). The upper one behaves as free fermions, whereas the lower branch, broad in energy, drops with increasing momentum. The first one can be attributed to the unpaired atoms, while the second one should come from molecules. The reduction in energy is due to the extra cost to dissociate a molecule. Therefore the energy offset should equal to the molecular binding energy. The negative effective mass reflects that molecules with higher binding energy occupies higher momentum component.

5 Discussion and conclusion

The BEC-BCS crossover regime provides rich physics. The exciting researches that have not been covered in this paper include the study on the spin-imbalanced case [14], and even a possible approach to study the pseuedogap region in high-temperature superconductor [15, 16]. Besides, the technique on probing physical properties in ultracold systems is blooming in recent years, and therefore the debating issues in condensed matter physics may find their solutions in this platform. In my opinion, in terms of the study on BEC-BCS crossover, we need to find more convincing methods to identify the Cooper-pair-like condensate.

In summary, from the BCS wavefunction, I displayed the basic properties of BEC-BCS

crossover at zero temperature. It indicates that by modifying the two-body interaction, the BCS-like Fermionic pairs in momentum space can become tightly bound molecules in real space. In ultracold Fermionic gas, the BEC-BCS crossover region can be realized through Feshbach resonance, which tunes the effective interaction between atoms by external magnetic field. The experimental results clearly demonstrated the existence of condensation on both sides, and displayed the corresponding momentum distribution under different temperature or detuning magnetic field. Moreover, the photoemission spectroscopy presented the information about the dispersion relationship, providing deeper insight into this problem.

References

[1] Anderson, M. H., J. R. Ensher, M. R. Matthews, C. E. Wieman, and E. A. Cornell, 1995, Science 269, 198.

[2] Davis, K. B., M.-O. Mewes, M. R. Andrews, N. J. van Druten, D. S. Durfee, D. M. Kurn, and W. Ketterle, 1995, Phys. Rev. Lett. 75, 3969.

[3] DeMarco, B., and D. D. Jin, 1999, Science 285, 1703.

[4] Eagles, D. M., 1969, Phys. Rev. 186, 456.

[5] Leggett, A. J., 1980, in Modern Trends in the Theory of Condensed Matter, edited by A. Pekalski and J. Przystawa Springer, Berlin.

[6] C. J. Pethick and H. Smith, Bose-Einstein Condensation in Dilute Gases, 2nd Edition. 2008, Cambridge.

[7] S. Giorgini, L. P. Pitaevskii and S. Stringari, 2008, Rev. Mod. Phys. 80, 1215.

[8] C. Chin, R. Grimm, P. Julienne and E. Tiesinga, 2010, Rev. Mod. Phys. 82, 1225.

[9] C. A. Regal, C. Ticknor, J. L. Bohn and D. S. Jin, 2003, Nature 424, 47.

[10] M. Greiner, C. A. Regal, and D. S. Jin, 2003, Nature 426, 537.

[11] M.W. Zwierlein, C. A. Stan, C. H. Schunck, S.M. F. Raupach, A. J. Kerman, and W. Ketterle, 2004. Phys. Rev. Lett. 92, 120403.

[12] C. A. Regal, M. Greiner, and D. S. Jin, 2004. Phys. Rev. lett. 92, 040303.

[13] J. T. Stewart1, J. P. Gaebler1 & D. S. Jin, 2008. Nature 454, 744.

[14] M. W. Zwierlein, A. Schirotzek, C. H. Schunck and W. Ketterle, 2006. Science 311, 492.

[15] J. P. Gaebler, J. T. Stewart, T. E. Drake, D. S. Jin, A. Perali, P. Pieri and G. C. Strinati, 2010. Nat. Phys. 6, 569.

[16] M. Feld, B. Frohlich, E. Vogt, M. Koschorreck & M. Kohl, 2011. Nature 480, 75.